

Constraints on the abundance of supermassive primordial black holes from lensing of compact radio sources

Huan Zhou,¹ Yujie Lian,² Zhengxiang Li,^{2*} Shuo Cao^{2†} and Zhiqi Huang¹

¹*School of Physics and Astronomy, Sun Yat-sen University, Zhuhai, 519082, China*

²*Department of Astronomy, Beijing Normal University, Beijing 100875, China*

Accepted XXX. Received YYY; in original form ZZZ

ABSTRACT

The possibility that primordial black holes (PBHs) form a part of dark matter has been considered over a wide mass range from the Planck mass (10^{-5} g) to the level of the supermassive black hole in the center of the galaxy. Primordial origin might be one of the most important formation channel of supermassive black holes. We propose the lensing effect of very long baseline interferometer observations of compact radio sources with extremely high angular resolution as a promising constraint on the abundance of intergalactic PBHs in the mass range $\sim 10^4$ - $10^9 M_{\odot}$. For a sample of well-measured 543 flat-spectrum compact radio sources, no milli-lensed images are found with angular separations between 1.5 milli-arcseconds and 50 milli-arcseconds. From this null search result, we derive that the fraction of dark matter made up of supermassive PBHs in the mass range $\sim 10^6$ - $10^8 M_{\odot}$ is $\lesssim 0.56\%$ at 68% confidence level. This constraints would be significantly improved due to the rapid increase of the number of measured compact radio sources.

Key words: Supermassive primordial black holes, Compact radio sources, Gravitational lensing

1 INTRODUCTION

The cosmological constant plus cold dark matter (Λ CDM) model has explained the evolution of the universe successfully. The scenario where CDM accounts for about a quarter of the total energy density is well consistent with current cosmological observations. However, we still know little about the constituent of dark matter (DM). Primordial black holes (PBHs) (Hawking 1971; Carr & Hawking 1974; Carr 1975), which are predicted to form in the infant universe via different mechanisms, such as the enhanced curvature perturbations during inflation (Clesse & García-Bellido 2015; Pi et al. 2018; Ashoorioon et al. 2021; Fu et al. 2019; Chen & Cai 2019; Motohashi et al. 2020), bubble collisions (Hawking et al. 1982), cosmic string (Hogan 1984; Hawking 1989), and domain wall (Caldwell et al. 1996), have been considered to be a promising candidate for the long elusive missing DM and therefore been a source of interest for nearly half a century. More interestingly, (stellar mass) PBHs have been attracting particular attention since the first detection of gravitational wave (GW) signal from the merger of black hole binary (Abbott et al. 2016). This signal also can be interpreted as ripples of spacetime from the merger of PBH binary (Bird et al. 2016; Sasaki et al. 2016; Clesse & García-Bellido 2017a).

So far, numerous methods have been proposed to constrain the abundance of PBHs, usually quoted as the frac-

tion of PBHs in DM $f_{\text{PBH}} = \Omega_{\text{PBH}}/\Omega_{\text{DM}}$ at present universe, in various possible mass windows including direct observational effects: gravitational lensing (Kassiola et al. 1991; Alcock et al. 2001; Wilkinson et al. 2001; Tisserand et al. 2007; Griest et al. 2013; Mediavilla et al. 2017; Zumalacarregui & Seljak 2018; Niikura et al. 2019,a; Liao et al. 2020; Zhou et al. 2021a,b), dynamical effects on ultrafaint dwarf galaxies (Brandt 2016; Koushiappas & Loeb 2017), disruption of white dwarfs (Graham et al. 2015), the effect of accretion via cosmic microwave background observations (Chen et al. 2016; Ali-Haimoud, & Kamionkowski 2017; Aloni et al. 2017; Poulin et al. 2017; Bernal et al. 2017), nondetections of stochastic GW from binary black holes (Clesse & García-Bellido 2017b; Wang et al. 2018; Chen & Huang 2020; De Luca et al. 2020; Hütsi, et al. 2021), (extra)galactic γ -ray backgrounds (Carr et al. 2016; DeRocco & Graham 2019; Laha 2019; Laha et al. 2020), and indirect observational effects: null detection of scalar-induced GW (Chen et al. 2019), cosmic microwave background (CMB) spectral distortions from the primordial density perturbations (Carr & Lidsey 1993; Carr et al. 1994). In addition to these available probes, some other constraints from the near future observations, such as gravitational lensing of GW (Diego 2020; Liao et al. 2020), gamma-ray bursts (Ji et al. 2018), and 21 cm signals (Hektor et al. 2018; Clark et al. 2018; Halder & Banerjee 2021), have been proposed. See Sasaki et al. (2018); Green & Kavanagh (2021) for a recent review.

In addition to stellar or much smaller mass ranges, PBHs are also appealing for investigating the issue of supermassive

* E-mail: zxli918@bnu.edu.cn

† E-mail: caoshuo@bnu.edu.cn

black holes (SMBHs) observed at very high redshifts. For instance, observations of quasars at $z \geq 6$ indicate that SMBH with masses greater than $\sim 10^9 M_\odot$ (Yang et al. 2020), which are challenging to be formed via some astrophysical processes (Woods et al. 2019). That is, the formation mechanism of SMBH is still a mystery in astrophysics. Actually, even assuming that the black hole continues the Eddington-limited accretion, it is nearly impossible for stellar-mass black holes ($\sim 10 - 1000 M_\odot$) growing to reach the mass of $\sim 10^9 M_\odot$ during the lifetime of the universe at $z \simeq 6$. Moreover, it is also not yet clear if such an efficient accretion can persistently operate for cases from stellar-mass black holes to SMBHs within the Hubble time. Therefore, PBHs as progenitor of SMBHs are an alternative possibility and have been widely studied in the literature (Duechting 2004; Kawasaki et al. 2012; Nakama et al. 2016; Hasegawa & Kawasaki 2018; Kawasaki & Murai 2019; Kitajima & Takahashi 2020). However, it is known that if PBHs with masses $10^4 - 10^{13} M_\odot$ are assumed to originate from the Gaussian primordial curvature perturbation, such primordial perturbations ineluctably result in the spectral distortion of the CMB which significantly exceeds the upper limit obtained by the COBE/FRIAS experiment (Kohri et al. 2014). Therefore, a scenario with highly non-Gaussian perturbations has been proposed to create PBHs (Kohri et al. 2014; Nakama et al. 2016; Huang 2019; Shinohara et al. 2021). This formation mechanism predicts inevitable clustering of PBHs. In this case, direct probe for PBHs in the mass range $\sim 10^2 - 10^9 M_\odot$ using the lensing effect of very long baseline interferometer (VLBI) observations of compact radio source (CRS) with extremely high angular resolution would be a crucial test of the scenario where PBHs can explain SMBHs at high redshifts.

In this paper, we first apply the method of optical depth to constrain the abundance of PBHs with well-measured 543 CRSs, observed by a well-known VLBI survey undertaken by Preston et al. (1985) (hereafter P85). Benefit from the high-quality maps obtained by VLBI, one is able to measure the milli-arcsecond ultra-compact structure in radio sources (Kellermann 1993) and search possible examples of multiple images produced by milli-lensing. Based on the null search result with updated redshift measurements of P85 (Jackson & Jannetta 2006), we obtain the most stringent limit on the abundance of supermassive primordial black holes (SMPBHs) in the mass range $\sim 10^6 - 10^8 M_\odot$.

This paper is organized as follows: we introduce the CRS data and the theory of optical depth of CRS lensing in Section 2. In Section 3, we apply this method to the CRS observations and yield results. Conclusions and discussions are presented in Section 4. Throughout, we use the concordance Λ CDM cosmology with the best-fit parameters from the recent Planck observations (Planck Collaboration, 2020).

2 METHODOLOGY

In this section, we briefly introduce current data of CRS observations and the optical depth theory of CRS lensing based on the method from Press & Gunn. (1973); Kassiola et al. (1991); Wilkinson et al. (2001).

2.1 Compact Radio Source Observations

The parent data used in this paper was derive from a catalog of ultra-compact radio sources, based on the observations of a 2.29 GHz VLBI all-sky survey (Preston et al. 1985). By employing a intercontinental VLBI array with an effective baseline of $\sim 8 \times 10^7$ wavelengths, 917 sources have been systematically observed with compact structure out of 1398 known radio sources. Note that these detected extragalactic objects coincide with different optical counterparts such as BL Lac objects, quasars, and radio galaxies (Gurvits 1994; Gurvits, Kellerman & Frey 1999; Cao et al. 2015), with a correlated flux limit of approximately 0.1 Jy. In this analysis, we focus on a revised sample including a significant fraction of P85 catalog, with updated redshift measurements and radio information for 613 objects covering the redshift range of $0.0035 \leq z \leq 3.787$. The full description of the observations and the corresponding details (i.e., source name, angular size of the compact structure, total radio flux density, spectral index, and optical counterpart) can be found in (Preston et al. 1985; Jackson & Jannetta 2006)¹. Such data has been extensively investigated in a number of cosmological studies, focusing on its possibility of establishing a sample of standard cosmological rulers at higher redshifts (Jackson 2004; Cao et al. 2017a,b, 2018; Qi et al. 2019, 2021). On the other hand, it is well known that radio-loud active galactic nuclei (AGN) typically contains a flat-spectrum core and a steep-spectrum jet. In the framework of core-jet model proposed by Blandford & Königl (1979), flat-spectrum radio sources could be explained as the stationary compact ends of quasi-steady supersonic jets, which always appear as the brightest unresolved compact cores in the VLBI images. Therefore, following the analysis of Gurvits, Kellerman & Frey (1999), we also apply a selection criterion to define the so-called “flat-spectrum core”, with spectral index $\alpha \geq -0.5$. In this context, the spectra index is defined as $S \propto \nu^\alpha$, where S is the flux density and ν is the frequency. The redshift distribution for the final CRS sample ($N = 543$), which contains all of the strongest flat-spectrum compact radio sources in P85 VLBI survey, is shown in Fig. 1.

In order to carry out systematic search for strong gravitational lenses on mas-scales, with possible multiple images produced by gravitational lensing, we turn to the Astrogeo VLBI FITS image database², the NASA/IPAC Extragalactic Database (NED)³, and the VLBI-derived catalogue OCARS⁴ (Malkin 2018) to obtain the radio images and additional information of these 543 flat-spectrum CRSs. Specially, the B1950 and J2000 name for the P85 radio sources are determined at the Astrogeo VLBI FITS image database at the time this search, with the source name, positions and redshift given by Preston et al. (1985). It is worth noting that the final CRS sample ($N = 543$) were observed at multiple radio frequencies, showing an unresolved flat-spectrum core with high resolution in at least one of the available observing band. The presence of two or more flat-spectrum core images provides a simple and interesting probe to detect candidates of lensed CRSs, with massive PBHs acting as point-like lenses. We try

¹ A full list is available via <http://nrl.northumbria.ac.uk/13109/>.

² http://astrogeo.org/vlbi_images/.

³ <http://ned.ipac.caltech.edu/>.

⁴ http://www.gaoran.ru/english/as/ac_vlbi/ocars.txt.

to find suitable lens candidates from the 543 flat-spectrum CRSs, based on the three major selection criteria as mentioned in Wilkinson et al. (2001): I) For the surface-brightness distribution of CRS, the primary compact component should be much larger than the secondary and other counterparts; II) For the flux density of the CRS, the ratio of the primary and secondary compact components should be $\leq 40 : 1$; III) For the positions of the CRS cores, the separation of the primary and secondary compact components should be $\delta \leq \Delta\theta \leq \Delta$. Here δ and Δ denote the minimum and maximum image separations, i.e., the angular resolution and the limited field of view (FoV) of the observation with which each radio source was observed. In this analysis we make a conservative estimation and take the typical value of $\delta = 1.5$ mas (the achievable resolution with the visibility distribution of the VLBI core) and $\Delta = 50$ mas (the field of view of $\sim 50 \times 50$ mas) for the P85 radio sources (Wilkinson et al. 2001).

At the first stage, we visually inspect all of the radio sources in all available frequencies searching for images with multiple compact components on mas-scales. After a careful check of the final CRS sample, 43 sources were selected, showing multiple compact components in at least one of the available bands. Now we report a few extra notes and considerations on all of the possible lensed sources. I) 31 candidates are confirmed to be core-jet sources, where the radio image exhibits a bright core and a faint jet with lower brightness hot-spot. This directly allows us to discard them as a lenses. II) 3 candidates turn out to be Compact Symmetric Objects (CSOs), which often show a single central core straddled by a pair of outer lobes of significantly lower surface brightness (Fanti et al. 1995; Readhead et al. 1996). The corresponding orders of these three sources in P85 catalog are 982, 1062, and 1076, while the J2000 names of these sources are J1558-1409, J1723-6500, and J1734+0926 (Sokolovsky et al. 2011; Angioni et al. 2019; An et al. 2012). It is interesting to note that J1558-1409 has been identified as a CSO candidate but not a confirmed one (Sokolovsky et al. 2011). However, compared with the 2 GHz radio images, its 8 GHz radio image reveals a new component between the two main ones, suggesting that the structure consists of a bright core and knots in a faint underlying lobe. III) 4 sources J0956+2515, J1357+4353, J2247-1237, and J2354-0019, whose orders are 567, 865, 1308, and 1384 in P85 catalog are rejected on account of at least one of the three basic selection criteria. For instance, J1357+4353 has also been identified as a CSO candidate by the recent work of Sokolovsky et al. (2011), in which the flux density ratios between the two compact component (1.512 ± 0.111 at 2 GHz and 2.208 ± 0.235 at 8 GHz) were reported. Considering the criterion that the lensed images should have identical radio spectra, or equivalently consistent flux ratio at different frequencies, such source is excluded as a lens because of its inconsistent multi-frequency flux ratios. IV) For 4 candidates: J0008-2339, J1101+7225, J1809+2758, and J1939-1002 (whose orders are 9, 647, 1105, and 1148 in P85 catalog), the weaker secondary component is not detected at a different observing frequency, or its surface brightness is much lower than the compact primary counterpart. Although the nature of the secondary component is still a controversy, it is less possible to be a the other lensed image of compact component on mas-scale. V) For the source J1107-6820 with the order of 661 in P85 catalog, Ojha et al. (2005) has reported the VLBI 8.4 GHz radio image and flux density ratio between

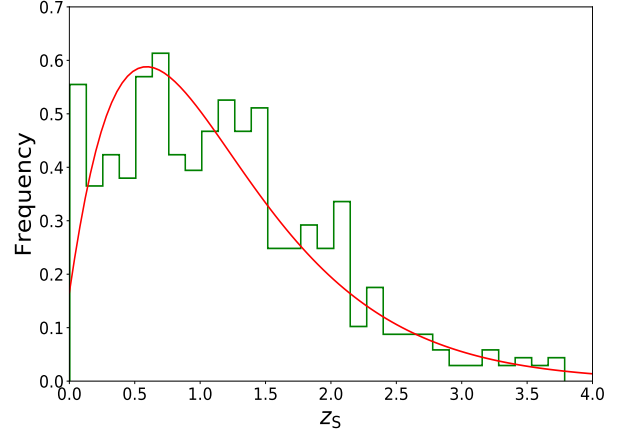


Figure 1. Redshift distribution of well-measured 543 CRSs.

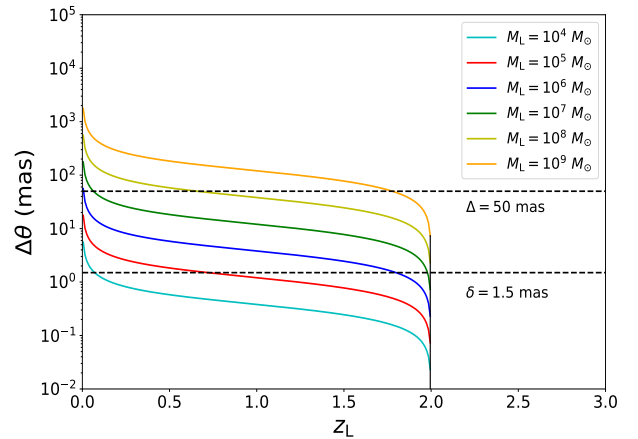


Figure 2. The angular separation of two images as a function with respect to the redshift of the lens, for a source at redshift $z_S = 2$. The mass of the lens ranges from 10^4 to $10^9 M_\odot$. The magnifications ratio of the images is $R_f = 40$.

the two compact components of J1107-6820. However, with the absence of radio images and flux density measurements at different frequencies, we fail to confirm its possibility to pass the follow-up tests and act as a milli-lensed candidate. Therefore, no strong evidence of milli-lensed candidate is found for the 543 flat-spectrum CRSs. Such conclusion is well consistent with the recent results of Casadio et al. (2021), focusing on the search of probable milli-lensed candidates based on a sample of 13828 individual sources from Astrogateo. It is worth noting that the two candidates, with a higher probability of being associated with gravitational lenses are not included in our P85 CRS sample.

2.2 Lensing of Compact Radio Sources

For a point mass M_{PBH} lens, Einstein radius is

$$\theta_E = 2\sqrt{\frac{GM_{\text{PBH}}}{c^2 D}} \approx (1 \text{ mas}) \left(\frac{M_{\text{PBH}}}{10^5 M_\odot} \right)^{1/2} \left(\frac{D}{\text{Gpc}} \right)^{-1/2}, \quad (1)$$

where G and c denote the gravitational constant and the speed of light, respectively. In addition, $D = D_L D_S / D_{LS}$ is effective lensing distance, where D_S , D_L , and D_{LS} represent the angular diameter distance to the source, to the lens, and between the source and the lens, respectively. The angular resolution for some CRSs with very long baseline array (VLBA) could reach a high level, e.g. \sim mas, it is possible to distinguish multiple images of an CRS lensed by intervening objects with mass greater than $\sim 10^5 M_\odot$. Because the Schwarzschild radius of PBH is much smaller than the Einstein radius multiplied by the angular diameter distance of the lens, i.e. $R_{\text{PBH}} = 2GM_{\text{PBH}}/c^2 \ll \theta_E D_L$, the lens equation of a point mass M_{PBH} is

$$\theta^2 - \beta\theta - \theta_E^2 = 0, \quad (2)$$

where β stands for the source position. The above lens equation of a point mass lens means there would be two images at positions

$$\theta_\pm = \frac{1}{2} \left(\beta \pm \sqrt{\beta^2 + 4\theta_E^2} \right). \quad (3)$$

It is obvious that one image locates outside the Einstein ring with $\theta_+ > \theta_E$ and the other one is within the ring $\theta_- < \theta_E$. Their magnifications μ_\pm satisfy

$$\mu_\pm = \left(1 - \frac{\theta_E^4}{\theta_\pm^4} \right)^{-1}. \quad (4)$$

In addition, the magnification ratio between two images can be directly obtained as well,

$$R_f \equiv \left| \frac{\mu_+}{\mu_-} \right| = \left| \frac{\theta_+}{\theta_-} \right|^4, \quad (5)$$

where the relation between two images $\theta_+ \theta_- = -\theta_E^2$ is used. The normalized impact parameter $y \equiv \frac{\beta}{\theta_E}$ for a reference value of magnification ratio R_f is

$$y(R_f) = R_f^{1/4} - R_f^{-1/4}. \quad (6)$$

In order to make both lensed images, especially the fainter one, detectable with high enough signal-noise ratio, R_f should be smaller than a threshold $R_{f,\text{max}}$. Following [Wilkinson et al. \(2001\)](#), we set the maximum value of magnification ratio $R_{f,\text{max}} = 40$.

The lensing cross section due to a PBH lens is given by

$$\sigma(M_{\text{PBH}}, z_L, z_S) = \frac{4\pi G M_{\text{PBH}} D_L D_{LS}}{c^2 D_S} [y_{\text{max}}^2(\Delta, M_{\text{PBH}}, z_L, z_S) - y_{\text{min}}^2(\delta, M_{\text{PBH}}, z_L, z_S)], \quad (7)$$

where the maximum impact parameter $y_{\text{max}}(\Delta, M_{\text{PBH}}, z_L, z_S)$ and minimum impact parameter $y_{\text{min}}(\delta, M_{\text{PBH}}, z_L, z_S)$ are determined by the angular resolution δ and the FoV of the observation Δ , respectively. Meanwhile, the impact parameter must be smaller than $y_{\text{max}}(R_{f,\text{max}})$. Now, we explain the maximum and minimum impact parameter in the cross section. The angular

separation of two images lensed by a PBH is

$$\Delta\theta = \theta_E (R_f^{1/4} + R_f^{-1/4}). \quad (8)$$

Illustratively, as shown in [Fig. 2](#), for an CRS at redshift $z_S = 2$, imaged with a fixed $R_f = 40$, $\delta = 1.5$ mas, and $\Delta = 50$ mas, we have plotted the angular separation of the images against the redshift of the lens with different masses. It is obvious that the angular separation $\Delta\theta$ decreases as lens redshift z_L increases. For a source at $z_S = 2$ and small mass PBH lenses ($\lesssim 10^6 M_\odot$), the upper limit of the lens redshift producing two detectable images is truncated by the angular resolution δ (the lower dotted line in [Fig. 2](#)). While for large mass PBH lenses ($\gtrsim 10^7 M_\odot$), the lower limit of the lens redshift producing two detectable images is determined by the FoV Δ (the upper dotted line in [Fig. 2](#)). It is obvious that the upper bound of lens redshift is very close to the one of the source and lower bound is very close to zero within the mass range $10^6 \sim 10^7 M_\odot$.

If the angular resolution is δ , we only are able to detect the presence of lens mass M_{PBH} assuming an CRS is at redshift z_S when the value of angular separation of two images satisfy

$$\Delta\theta \geq \delta. \quad (9)$$

This requirement results in a minimum impact parameter $y_{\text{min}}(\delta, M_{\text{PBH}}, z_L, z_S)$. Analogously, we can only detect secondary images if they lie within the FoV of the observation, Δ . That is, the value of angular separation of two images must satisfy

$$\Delta\theta \leq \Delta. \quad (10)$$

This condition yields a maximum impact parameter $y_{\text{max}}(\Delta, M_{\text{PBH}}, z_L, z_S)$. For a given lens mass M_{PBH} and an CRS at redshift z_S , equation (10) will always be violated when the redshift of lens is smaller than z_Δ , a solution of $\Delta\theta = 2\theta_E = \Delta$. This violation heralds that the minimum angular separation of two images is larger than the FoV of the observation. Therefore, there is no contribution of cross section at redshifts smaller than z_Δ . Moreover, when the redshift of lens is between z_Δ and z_δ that comes from the $\Delta\theta = 2\theta_E = \delta$, the minimum angular separation of two images come in the range of FoV but is still larger than the angular resolution. In this case, the minimum impact parameter $y_{\text{min}}(\delta, M_{\text{PBH}}, z_L, z_S)$ must be zero. However, the maximum impact parameter $y_{\text{max}}(\Delta, M_{\text{PBH}}, z_L, z_S)$ can be derived from equation (10) as follows

$$y_{\text{max}}(\Delta, M_{\text{PBH}}, z_L, z_S) = \frac{\Delta/\theta_E + \sqrt{(\Delta/\theta_E)^2 - 4}}{2} - \frac{\Delta/\theta_E + \sqrt{(\Delta/\theta_E)^2 - 4}}{2}. \quad (11)$$

When the redshift of lens is larger than z_δ , the minimum impact parameter $y_{\text{min}}(\delta, M_{\text{PBH}}, z_L, z_S)$ can be derived equation (8) as

$$y_{\text{min}}(\delta, M_{\text{PBH}}, z_L, z_S) = \frac{\delta/\theta_E + \sqrt{(\delta/\theta_E)^2 - 4}}{2} - \frac{\delta/\theta_E + \sqrt{(\delta/\theta_E)^2 - 4}}{2}. \quad (12)$$

It should be pointed out that the method in [Kassiola et al. \(1991\)](#) for calculating the truncated redshifts leads to underestimate of cross section contribution from the low redshift

and the redshift close to the source. Therefore, for a single source, the lensing optical depth due to a single PBH lens should be

$$\begin{aligned} \tau(M_{\text{PBH}}, f_{\text{PBH}}, z_{\text{S}}) &= \int_0^{z_{\text{S}}} d\chi(z_{\text{L}})(1+z_{\text{L}})^2 n_{\text{L}}(f_{\text{PBH}}) \\ \sigma(M_{\text{PBH}}, z_{\text{L}}, z_{\text{S}}) &= \frac{3}{2} f_{\text{PBH}} \Omega_{\text{DM}} \int_0^{z_{\text{S}}} dz_{\text{L}} \frac{H_0^2}{cH(z_{\text{L}})} \frac{D_{\text{L}} D_{\text{LS}}}{D_{\text{S}}} \\ (1+z_{\text{L}})^2 [y_{\text{max}}^2(\Delta, M_{\text{PBH}}, z_{\text{L}}, z_{\text{S}}) - y_{\text{min}}^2(\delta, M_{\text{PBH}}, z_{\text{L}}, z_{\text{S}})], \end{aligned} \quad (13)$$

where n_{L} is the comoving number density of the lens, H_0 is the Hubble constant, $H(z_{\text{L}})$ is the Hubble parameter at z_{L} , and Ω_{DM} is the present fractional density of DM.

Now, for a given distribution function $N(z_{\text{S}})$ of CRSs, their integrated optical depth $\bar{\tau}(M_{\text{PBH}}, f_{\text{PBH}})$ is

$$\bar{\tau}(M_{\text{PBH}}, f_{\text{PBH}}) = \int dz_{\text{S}} \tau(M_{\text{PBH}}, f_{\text{PBH}}, z_{\text{S}}) N(z_{\text{S}}). \quad (14)$$

If one observes a large number of CRSs, N_{CRS} , then the number of detectable lensed CRSs is expected to be

$$N_{\text{lensed CRS}} = (1 - e^{-\bar{\tau}(M_{\text{PBH}}, f_{\text{PBH}})}) N_{\text{CRS}}. \quad (15)$$

If none of the CRS is found to be lensed, then the constraint on the upper limit of the fraction of DM in the form of PBHs can be estimated from equation (15).

3 RESULTS

We first use the optical depth method to constrain the abundance of SMPBHs. The common definition of strong lensing refers to images with a magnification ratio $R_{\text{f}} = 7$, our $R_{\text{max}, \text{f}} = 40$ magnification ratio corresponds to a configuration with a larger impact parameter and hence the lensing optical depth (cross section) is almost 5 times larger than that normally assumed for lensing calculations. Each source is observed with an approximately fixed angular resolution corresponding to the minimum image separation, $\delta = 1.5$ mas, and limited FoV, $\Delta = 50$ mas. The angular resolution and the limited FoV act to truncate the mass range of the lenses that produce detectable multiple images. The upper limit of the abundance of SMPBHs is insensitive to the angular resolution δ and FoV Δ . This inference is similar as the one concluded in [Kassiola et al. \(1991\)](#). If there is no truncation on mass, the comoving number density n of PBH with a particular mass is proportional to $1/M_{\text{PBH}}$ for a given value of f_{PBH} . In addition, the gravitational lensing cross section σ is $\propto M_{\text{PBH}}$, and hence the path length to lensing $1/(n\sigma)$ is independent on the lens mass. Thus, the optical depth across the measurable mass range is roughly a constant, yielding a universal upper limit of f_{PBH} . Our search is sensitive to the mass range from $\sim 10^6 M_{\odot}$ to $\sim 10^8 M_{\odot}$. In addition, within this lens mass range, the null search result of lensed CRSs leads to a constraint on the upper limit of f_{PBH} . As shown in Fig. 3, at the 68% confidence level, the fraction of DM in the form of SMPBHs with the mass ranging from $10^6 M_{\odot}$ to $10^8 M_{\odot}$ is $\lesssim 0.56\%$. Compared with the limits presented in [Wilkinson et al. \(2001\)](#), our constraint has been significantly improved quantitatively and qualitatively. The quantitative improvement arises from the optical depth method and the sample consisting of more sources (543, cf. 300). The

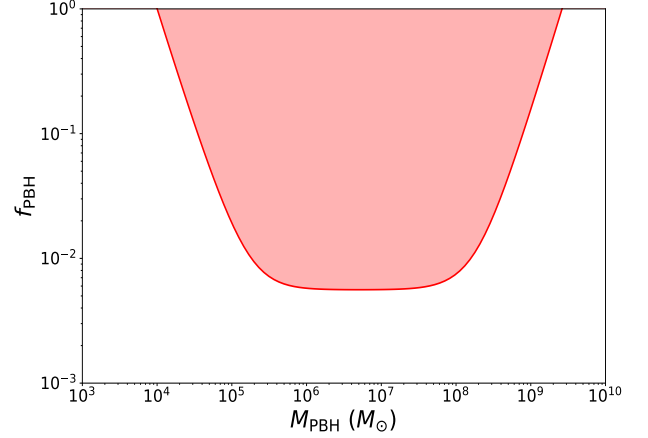


Figure 3. Constraint on f_{PBH} at the 68% confidence level from the null search result of lensing candidate with image separations in the range 1.5-50 mas in the well-measured 543 CRSs.

qualitative improvement is that we use the standard Planck best-fit Λ CDM model, in contrast of the Einstein-de Sitter universe ($\Omega_{\text{M}} = 1, \Omega_{\Lambda} = 0$) used in [Wilkinson et al. \(2001\)](#). These improved constraints would be helpful and complementary for probing the possibility of SMPBHs in this mass window making up DM.

4 CONCLUSIONS AND DISCUSSIONS

In this paper, we have proposed to constrain the presence of intergalactic PBHs in the mass range $\sim 10^4 - 10^9 M_{\odot}$ with the lensing effect of CRS which are observed by VLBI with extremely high angular resolution. By searching examples of multiple images produced by milli-lensing in a sample of well-measured 543 CRSs, no evidence of lensed candidates was found with angular separations in the range 1.5-50 milli-arcseconds. Based on the optical depth method, we derive the 68% confidence-level constraint on the fractional abundance of SMPBHs, $f_{\text{PBH}} < 0.56\%$, in the mass range $\sim 10^6 - 10^8 M_{\odot}$. This constraint might be conservative, because gravitational lensing effect increases the observed flux density of a background source. As a result, lensed sources are drawn from a fainter source population than the unlensed sources. In this case, a flux-limited survey will probably contain more lensed candidates than expected. Therefore, the null search result formally leads to a more stringent bound on f_{PBH} . This ‘‘magnification bias’’ associated with sources used in our analysis is of order unity.

We expect the constraint on f_{PBH} to be significantly improved in the near future. Assuming detection of $\sim 10^4$ unlensed CRSs with same redshift distribution, angular resolution and FoV ⁵ ([Casadio et al. 2021](#)), we find that uniformly distributed SMPBHs in the mass range from $\sim 10^6 M_{\odot}$ to $\sim 10^8 M_{\odot}$ do not make up more than $\sim 0.03\%$ of DM at the 68% confidence level.

The above direct constraints on SMPBH can provide clues

⁵ http://www.gaoran.ru/english/as/ac_vlbi/

about the origin of SMBHs. It is well known that the formation of black holes with masses greater than $\sim 10^9 M_{\odot}$ observed at $z \geq 6$ is still mysterious since the continuous Eddington-limited accretion is far insufficient for stellar-mass black holes growing to SMBHs during the life-time of the universe. PBHs have been widely proposed as seeds of SMBHs. Therefore, direct constraints from the well-measured 543 CRSs would be helpful for exploring this issue. Moreover, SMPBHs can form binaries, coalesce, and produce GWs in nano-Hertz frequency band, which can be detected by using stable millisecond pulsars (Jaffe & Backer 2003; Sesana et al. 2008, 2009). The null-detection of GWs by pulsar timing array (PTA) can successfully constrain continuous GWs from individual supermassive binaries black holes (Zhu et al. 2014; Babak et al. 2016; Aggarwal et al. 2019). It suggests that PTA experiment also is an important tool to constrain SMBHs in the near future. In combination of milli-lensing of CRSs and measurement of continuous GWs from individual supermassive binaries black holes, it is foreseen that upcoming complementary multi-messenger observations will yield considerable constraints on the possibilities of SMPBHs.

ACKNOWLEDGEMENTS

This work was supported by the National Natural Science Foundation of China under Grants Nos. 11920101003, 11722324, 11603003, 11633001, 12073088, and U1831122; National Key R&D Program of China No. 2017YFA0402600; Guangdong Major Project of Basic and Applied Basic Research (Grant No. 2019B030302001); the Strategic Priority Research Program of the Chinese Academy of Sciences, Grant No. XDB23040100, and the Interdiscipline Research Funds of Beijing Normal University.

DATA AVAILABILITY

The data underlying this article will be shared on reasonable request to the corresponding author.

REFERENCES

Abbott, B. P., Abbott, R., Abbott, T. D., et al., 2016, PRL, 116, 061102
 Aggarwal, K., Arzoumanian, Z., Baker, P. T., et al., 2019, ApJ, 880, 116
 Aghanim, N., Akrami, Y., Ashdown, M., et al., 2020, A&A 641, A6
 Alcock, C., Allsman, R. A., Alves, D. R., et al., 2001, ApJ, 550, L169
 Ali-Haïmoud Y., Kamionkowski M., 2017, PhRvD, 95, 043534
 Aloni, D., Blum, K., Flauger, R., 2017, JCAP, 05, 017
 An, T., Wu, F., Yang, J., et al., 2012, ApJS, 198, 5
 Angioni, R., Ros, E., Kadler, M., et al., 2019, A&A, 627, A148
 Ashoorioon, A., Rostami, A., Firouzjaee, J. T., 2021, JHEP, 07, 087
 Babak, S., Petiteau, A., Sesana, A., et al., 2015, MNRAS, 455, 1065
 Bernal, J. L., Bellomo, N., Raccanelli, A., Verde, L., 2017, JCAP, 10, 052
 Bird, S., Cholis, I., Muñoz, J. B., Ali-Haïmoud, Y., Kamionkowski, M., 2016, PRL, 116, 201301

Blandford, R. D., Königl, A., 1979, ApJ, 232, 34
 Brandt, T. D., 2016, ApJ, 824, L31
 Caldwell, R. R., Chamblin, A., Gibbons, G. W., 1996, PRD, 53, 7103
 Cao, S., Biesiada, M., Zheng, X., Zhu, Z.-H., 2015a, ApJ, 806, 66
 Cao, S., Biesiada, M., Jackson, J., Zheng, X.-G., Zhao, Y.-H., 2017a, JCAP, 02, 012
 Cao, S., Zheng, X.-G., Biesiada, M., et al., 2017b, A&A, 606, A15
 Cao, S., Biesiada, M., Qi, J.-Z., et al., 2018, EPJC, 78, 749
 Carr, B. J., Hawking, S. W., 1974, MNRAS, 168, 399
 Carr, B. J., 1975, ApJ, 201, 1
 Carr, B. J., Lidsey, J. E., 1993, PRD, 48, 543
 Carr, B. J., Gilbert, J. H., Lidsey, J. E., 1994, PRD, 50, 4853
 Carr, B. J., Kohri, K., Sendouda, Y., Yokoyama, J., 2016, PRD, 94, 044029
 Casadio, C., Blinov, D., Readhead, A. C. S., et al., 2021, MNRAS, 507, L6
 Chen, L., Huang, Q.-G., Wang, K., 2016, JCAP, 12, 044
 Chen, C., Cai, Y.-F., 2019, JCAP, 10, 068
 Chen, Z.-C., Yuan, C., Huang, Q.-G., 2020, PRL, 124, 251101
 Chen, Z.-C., Huang, Q.-G., 2020, JCAP, 08, 039
 Clark, S., Dutta, B., Gao, Y., Ma, Y.-Z., Strigari, L. E., 2018, PRD, 98, 043006
 Clesse, S., García-Bellido, J., 2015, PRD, 92, 023524
 Clesse, S., García-Bellido, J., 2017a, Phys. Dark Univ. 15, 142
 Clesse, S., García-Bellido, J., 2017b, Phys. Dark Univ. 18, 105
 De Luca, V., Franciolini, G., Pani, P., Riotto, A., 2020, JCAP, 06, 044
 DeRocco, W., Graham, P. W., 2019, PRL, 123, 251102
 Diego, J. M., 2020, PRD, 101, 123512
 Duechting, N., 2004, PRD, 70, 064015
 Fanti, C., Fanti, R., Dallacasa, D., Schilizzi, R. T., Spencer, R. E., Stanghellini, C., 1995, A&A, 302, 317
 Fu, C.-J., Wu, P.-X., Yu, H.-W., 2019, PRD, 100, 063532
 Graham, P. W., Rajendran, S., Varela, J., 2015, PRD, 92, 063007
 Green, A. M., Kavanagh, B. J., 2021, J.Phys.G, 48, 043001
 Griest, K., Cieplak, A. M., Lehner, M. J., 2013, PRL, 111, 181302
 Gurvits, L. I., 1994, ApJ, 425, 442
 Gurvits, L. I., Kellerman, K. I., Frey, S., 1999, A&A, 342, 378
 Halder, A., Banerjee, S., 2021, PhRvD, 103, 063044
 Hasegawa, F., Kawasaki, M., 2018, PRD, 98, 043514
 Hawking, S. W., 1971, MNRAS, 152, 75.
 Hawking, S. W., Moss, I. G., Stewart, J. M., 1982, PRD, 26, 2681
 Hawking, S. W., 1989, PLB, 231, 237
 Hektor, A., Hutsi, G., Marzola, L., Raidal, M., Vaskonen, V., Veermäe, H., 2018, PRD, 98, 023503
 Hogan, C. J., 1984, PLB, 143, 87
 Huang, Z.-Q., 2019, PRD, 99, 103537
 Hütsi, G., Raidal, M., Vaskonen, V., Veermäe, H., 2021, JCAP, 03, 068
 Jackson, J. C., 2004, JCAP, 11, 007
 Jackson, J. C., Jannetta, A. L., 2006, JCAP, 11, 002
 Jaffe, A. H., Backer, D. C., 2003, ApJ, 583, 616
 Ji, L., Kovetz, E. D., Kamionkowski, M., 2018, PRD, 98, 123523
 Kassiola, A., Kovner, I., Blandford, B. D., 1991, ApJ, 358, 5
 Kawasaki, M., Kusenko, A., Yanagida, T. T., 2012, PLB, 711, 1
 Kawasaki, M., Murai, K., 2019, PRD, 100, 103521
 Kellermann, K. I., 1993, Nature, 361, 134
 Kitajima, N., Takahashi, F., 2020, JCAP, 11, 060,
 Kohri, K., Nakama, T., Suyama, T., 2014, PRD, 90, 083514
 Koushiappas, S. M., Loeb, A., 2017, PRL, 119, 041102
 Laha, R., 2019, PRL, 123, 251101
 Laha, R., Muñoz, J. B., Slatyer, T. R., 2020, PRD, 101, 123514
 Liao, K., Zhang, S.-B., Li, Z., Gao, H., 2020, ApJL, 896, L11
 Liao, K., Tian, S.-X., Ding, X.-H., 2020, MNRAS, 495, 2002
 Malkin, Z., 2018, ApJS, 239, 20
 Mediavilla, E., Jimenez-Vicente, J., Munoz, J. A., VivesArias, H., Calderon-Infante, J., 2017, ApJ, 836, L18

- Motohashi, H., Mukohyama, S., Oliosi, M., 2020, JCAP, 03, 002
 Nakama, T., Suyama, T., Yokoyama, J., 2016, PRD, 94, 103522
 Niikura, H., Masahiro, T., Naoki, Y., et al., 2019, Nature Astronomy, 3, 524.
 Niikura, H., Takada, M., Yokoyama, S., Sumi, T., Masaki, S., 2019, PRD, 99, 083503
 Nemiroff, R. J., 1989, ApJ, 341, 579
 Ojha, R., Fey, A. L., Charlot, P., et al., 2005, AJ, 130, 2529
 Pi, S., Zhang, Y.-L., Huang, Q.-G., Sasaki, M., 2018, JCPA, 1805, 42
 Poulin, V., Serpico, P. D., Calore, F., Clesse, S., Kohri, K., 2017, PRD, 96, 083524
 Press, W. H., Gunn, J. E., 1973, ApJ, 185, 397
 Preston, R. A., Morabito D. D., Williams J. G., et al., 1985, AJ, 90, 1599
 Qi, J.-Z., Cao, S., Zhang, S.-X., et al., 2019, MNRAS, 483, 1104
 Qi, J.-Z., Zhao, J.-W., Cao, S., Biesiada, M., Liu, Y.-T., 2021, MNRAS, 503, 2179
 Readhead, A. C. S., Taylor, G. B., Xu, W., Pearson, T. J., Wilkinson, P. N., Polatidis, A. G., 1996, ApJ, 460, 612
 Sasaki, M., Suyama, T., Tanaka, T., Yokoyama, S., 2016, PRL, 117, 061101
 Sasaki, M., Suyama, T., Tanaka, T., Yokoyama, S., 2018, GReGr, 35, 063001
 Sesana, A., Vecchio, A., Colacino, C. N., 2008, MNRAS, 390, 192
 Sesana, A., Vecchio, A., Volonteri, M., 2009, MNRAS, 394, 2255
 Shinohara, T., Suyama, T., Takahashi, T., 2021, PRD, 104, 023526
 Sokolovsky, K. V., Kovalev, Y. Y., Pushkarev, A. B., Mimica, P., Perucho, M., 2011, A&A, 535, A24
 Tisserand, P., Guillou, P., Afonso, C., et al., 2007, A&A 469, 387
 Wang, S., Wang, Y.-F., Huang, Q.-G., Li, T. G. F., 2018, PRL, 120, 191102
 Wilkinson, P. N., Henstock, D. R., Browne, W. A., et al., 2001, PRL, 86, 4
 Woods, T. E., Agarwal, B., Bromm, V., et al., 2019, PASA, 36, e027
 Yang, J., Wang, F., Fan, X., et al., 2020, ApJ, 897, L14
 Zhou, H., Li, Z.-X., Huang, Z.-Q., Gao, H., Huang, L., 2021, arXiv:2103.08510
 Zhou, H., Li, Z.-X., Liao, K., Niu, C.-H., Gao, H., Huang, Z.-Q., Huang, L., Zhang, B., 2021, arXiv: 2109.09251
 Zhu, X.-J., Hobbs, G., Wen, L. et al., 2014, MNRAS, 444, 3709
 Zumalacarregui, M., & Seljak, U., 2018, PRL, 121, 141101